Available online at www.sciencedirect.com

SciVerse ScienceDirect

Ceramics International 39 (2013) 4125–4132

CERAMICS INTERNATIONAL

www.elsevier.com/locate/ceramint

Ceramic pigments based on chromium doped alkaline earth titanates

A. García, R. Galindo, C. Gargori, S. Cerro, M. Llusar, G. Monrós*

Department of Inorganic and Organic Chemistry, Jaume I University, Av. de Vicent Sos Baynat, s/n. 12071 Castellón, Spain

Received 2 October 2012; received in revised form 29 October 2012; accepted 30 October 2012
Available online 16 November 2012

Abstract

In this paper $M(Ti_{1-x}Cr_x)O_3$ with M=Mg, Ca, Sr, Ba and $x=0.01$, 0.03, 0.05, 0.1 compositions have been prepared by solid state reaction in order to analyze their reactivity, structure, limit of solid solution, stability and pigmenting properties in conventional ceramic glazes. Cr–$MgTiO_3$ crystallizes magnesium ilmenite $MgTiO_3$ (SG=R-3) with residual $MgCr_2O_4$ spinel that inhibits the Cr entrance in solid solution and do not show pigmenting properties. Cr–$CaTiO_3$ crystallizes orthorhombic perovskite (SG=Pbnm) pink solid solutions associated to Cr^{4+}–Ti^{4+} substitutions which above $x=0.03$ unstabilizes in glazes and produce light green shades. Cr–$SrTiO_3$ crystallizes ideal cubic perovskite (SG=Pm3m) pink solid solutions that unstabilizes in glazes above $x=0.01$. Finally Cr–$BaTiO_3$ crystallizes tetragonal perovskite (SG=P4mn) with residual peaks of $BaCrO_4$ at $x=0.1$ showing pink solid solutions until $x=0.05$ that unstabilizes in glazes above $x=0.03$. All powders show aggregates (between 2–10 μm of size) of fine particles (between 200–1000 nm).

Keywords: D. Perovskites; Alkaline earth; Ceramic pigment; Chromium

1. Introduction

In the ideal cubic perovskite structure ABO_3 (SG=Pm3m) the little atom B occupies the center of a cube, the large atom A the corners and oxygen the face centers. The coordination number results VI (octahedral) for B and XII (cuboctahedral) for A. In agreement with Goldschmidt the relative ion size requirements for stability of the cubic structure are quite stringent: if purely ionic bonding is assumed, the degree of octahedral distortion parameter or Goldschmidt tolerance factor $t=(r_A+r_O)/[2^{1/2}(r_B+r_O)]$ must be between $0.78<t<1.05$ (where r_A is the ionic radius of A, r_B is the ionic radius of B, and r_O is the ionic radius of oxygen), the ideal cubic perovskite $SrTiO_3$ has $t=1.00$ (Pauling ionic radius $r_A=1.44$ Å, $r_B=0.605$ Å, and $r_O=1.40$ Å). If the value of t is 0.81 or less, the value of the A ion size is smaller than ideal, and the BO_6 octahedra will tilt in order to fill space. Since perovskites are not truly ionic compounds and since the t values also depend on what values are taken for the ionic radii, the tolerance factor is only a rough estimate. Thereby the introduction of d^9 (Cu^{2+}), d^4 high spin (Mn^{3+}) or d^7 low spin cations (Co^{2+}) produce a Jahn–Teller tetragonal distortion of BO_6 octahedra also. These distortions can produce a lower-symmetry version, in which the coordination numbers of A cations, B cations or both are reduced. In the case of low sized A cations, the tilting of the BO_6 octahedra reduces the coordination of A from XII to as low as VIII. Likewise, a low sized B cation within its octahedron attains a stable bonding pattern by loss of the central position of the octahedron. The resulting electric dipole is responsible for the property of ferroelectricity shown by perovskites such as $BaTiO_3$ that distort in this fashion [1]. $MgTiO_3$ is one of several ABO_3 compounds, including $FeTiO_3$, $MnTiO_3$, $MnSnO_3$, and $MgGeO_3$ that form ilmenite structure that transforms successively to a $LiNbO_3$ lithium niobate and perovskite structures at high pressures [2]. Ilmenite derives from corundum structure, in corundum all cations are identical but in ilmenite Fe^{2+} and Ti^{4+} ions occupy alternating layers perpendicular to the trigonal c axis. The unstability of the perovskite polymorphs possibly results from the comparatively small difference in radius of the A and B cations when compared to more stable perovskite compounds such as $CaTiO_3$ [3].

Recently [4–6] have been reported two new ceramic pigments based on chromium (pink) and vanadium (orange)

*Corresponding author. Tel.: +34 964 728250; fax: +34 964 728214.
E-mail address: monros@qio.uji.es (G. Monrós).

0272-8842/$ - see front matter © 2012 Elsevier Ltd and Techna Group S.r.l. All rights reserved.
http://dx.doi.org/10.1016/j.ceramint.2012.10.267

doped titanium–calcium perovskite The former is based on the solid solution of Cr^{4+} (0.55 pm) in $CaTiO_3$ lattice substuting Ti^{4+} (0.605 pm) [7]. When characterized its pigmenting properties by adding 5 wt% to a conventional glaze of the $CaO–ZnO–SiO_2$ system, the best coloration is obtained with 0.015 mol/mol of chromium in the composition and using a firing temperature of 1100 °C (CIEL*a*b* 59.3/12.5/9.5).

In this paper $M(Ti_{1-x}Cr_x)O_3$ with M = Mg, Ca, Sr, Ba and x = 0.01, 0.003, 0.005, 0.1 compositions have been prepared by solid state reaction in order to analyze the effect of the alkaline earth on the crystalline structure of the titanate ABO_3 and on their pigmenting properties in a conventional ceramic glaze matrix of the $CaO–ZnO–SiO_2$ system for double firing stoneware (1050 °C).

2. Experimental

$M(Ti_{1-x}Cr_x)O_3$ with M = Mg, Ca, Sr, Ba and x = 0.01, 0.03, 0.05, 0.1 compositions have been prepared by solid state reaction (ceramic route) from the alkaline earth carbonate and Cr_2O_3 and TiO_2 (anatase) oxides (all supplied by ALDRICH S.A.). The raw powders were fired successively at 1000 °C and 1200 °C with a soaking time of 3 h. Samples have been characterized by several techniques:

a) X-Ray Diffraction (XRD) carried out on a Siemens D5000 diffractometer using CuK_α radiation, 20°–70° 2θ range, scan rate 0.05° 2θ/s, 2 s per step and 40 kV and 20 mA conditions. Also for measuring the parameters of cell unit cell using α-Al_2O_3 as internal standard and indexation of XRD peaks by POWCAL and LSQC programmes [8], diffractogrammes at scan rate 0.01 °2θ/s, 5 s per step and 40 kV and 20 mA conditions were carried out.

b) Microstructure characterization of powders was carried out by Scanning Electron Microscopy (SEM), using a Leo-440i microscope supplied by LEYCA.

c) UV–vis–NIR spectra of 5% weight glazed samples in a conventional $SiO_2–CaO–ZnO$ glaze for a double firing stoneware (1050 °C) have been collected using a Jasco V670 spectrometer through diffuse reflectance technique. L*a*b* color parameters of glazed samples were measured following the CIE (Commission International de l'Eclairage) colorimetric method [9] using a X-Rite SP60 spectrometer, with standard lighting D65. On this method, L* is a measure of brightness (100 = white, 0 = black) and a* and b* of chroma (−a* = green, +a* = red, −b* = blue, +b* = yellow).

d) The thermal performance of the earth carbonates used have been analyzed in a DTA-TG (Differential Thermal Analysis-Thermogravimetric Analysis) Perkin Elmer TGA/SDTA851e/LF/1600 equipment using platinum crucibles and a firing speed of 5 °C/min from room temperature to 1200 °C.

3. Results and discussion

In the used ceramic method the precursors were homogenized in a planetary mill in acetone media. When acetone was evaporated the raw powders were fired successively at 1000 °C and 1200 °C with a soaking time of 3 h.

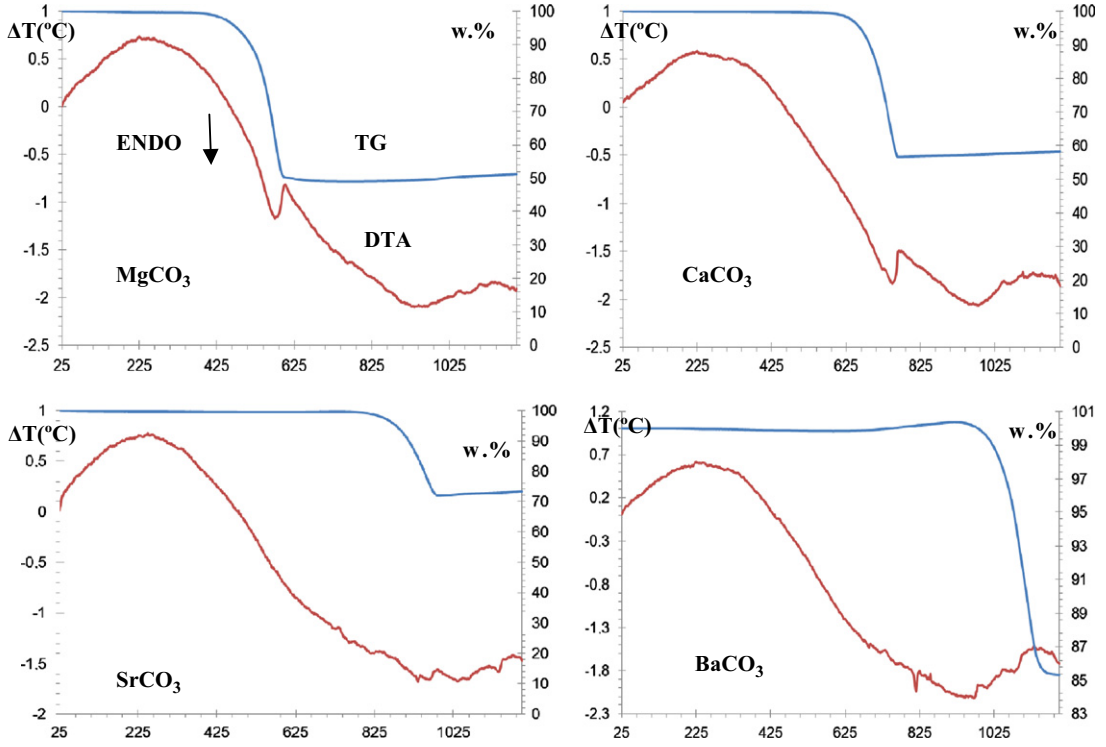

Fig. 1. DTA-TG with a firing speed of 5 °C/min from room temperature to 1200 °C of earth carbonates used as precursors.

DTA-TG with a firing speed of 5 °C/min from room temperature to 1200°C of earth carbonates used as precursors are shown in Fig. 1. A broad endothermic DTA band associated to a sharp mass loss could be observed at 570, 660, 950 and 1080 °C for $MgCO_3$, $CaCO_3$, $SrCO_3$ and $BaCO_3$ respectively which are associated to the respective carbonate decomposition. From these results, 1000 °C was chosen as the initial firing temperature in order to ensure decomposition of the carbonates (only $BaCO_3$ would remain at this temperature (Fig. 2).

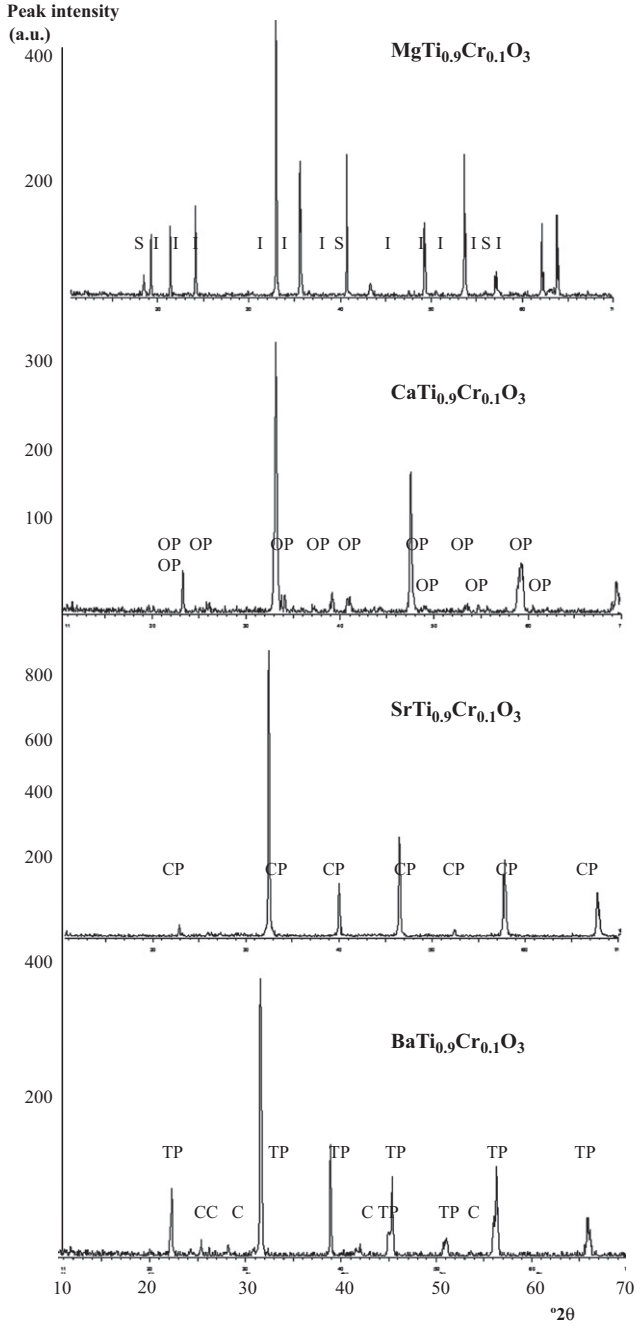

Fig. 2. XRD of samples $MTi_{0.9}Cr_{0.1}O_3$ fired at 1200 °C/3 h. Crystalline phases: I (Ilmenite $MgTiO_3$), S (Spinel $MgCr_2O_4$), OP (Orthorhombic perovskite $CaTiO_3$), CP (Cubic Perovskite $SrTiO_3$), TP (Tetragonal Perovskite $BaTiO_3$), C ($CaCrO_4$).

XRD results indicate that for $M=Ca^{2+}$ and Sr^{2+} samples fired at 1200 °C (Shannon effective radii of 1.48 and 1.58 Å in XII coordination respectively), the perovskite is the only crystalline phase detected, indicating that the chromium solid solution into $MTiO_3$ lattice is completed at 1200 °C (at 1000 °C $MCrO_4$ is detected by XRD in both samples). In agreement with the achievement of the solid solution, the lattice parameter measurements carried out in $Ca(Ti_{1-x}Cr_x)O_3$ perovskite (Fig. 3) indicate a gradual diminution of the unit cell volume of the perovskite with x following a Vegard linear variation [10].

$CaTiO_3$ crystallizes an orthorhombic perovskite (SG= Pbnm): the powders are pink colored in all x ranges, showing a red parameter $a^* > 10$ for all samples at 1200 °C. When the powder is 5% glazed (firing temperature of glaze=1050 °C), the pink color is observed until $x=0.03$ ($L^*a^*b^*=56.4/13.7/1.2$ for $x=0.03$) [3]. At higher x values Cr–$CaTiO_3$ produces green color in glazes ($L^*a^*b^*=64.5/-5.1/6.4$ for $x=0.1$).

$SrTiO_3$ crystallizes an ideal cubic perovskite (SG=Pm3m), the color of powders are pink in all range showing a valor $a^* > 10$ in all samples at 1200 °C, when the powder is 5% glazed (firing temperature of glaze=1050 °C) the pink color is observed only for $x=0.01$ ($L^*a^*b^*=66.2/8.6/15.1$). At higher x values Cr–$SrTiO_3$ produces yellow color in glazes ($L^*a^*b^*=62.4/-0.9/29.3$ for $x=0.1$).

With the small Mg^{2+} (Shannon effective radii of 0.86 Å) magnesium ilmenite structure $MgTiO_3$ (SG=R-3) is detected by XRD at 1200 °C together very weak peaks associated to $MgCr_2O_4$ spinel (at 1000 °C it is also detected with weak peaks of periclase MgO and karrooite $MgTi_2O_5$). The weak green powders do not have pigmenting properties in ceramic glazes.

Finally, the big Ba^{2+} (Shannon effective radii of 1.75 Å) crystallizes tetragonal perovskite (SG=P4mn) at 1200 °C with residual peaks associated to $BaCrO_4$ for $x=0.1$ sample (similar feature is observed a t 100 °C, see Table 1). The powders fired at 1200 °C are light pink (a^* around 5) until $x=0.05$. When the powder is 5% glazed (firing temperature of glaze 1050 °C) a light pink color is observed until $x=0.03$ ($L^*a^*b^*=66.2/5.6/26.6$ for $x=0.03$). At higher x values Cr–Ba TiO_3 give intense green–yellow color in glazes ($L^*a^*b^*=58.4/-1.1/43.9$ for $x=0.1$) (Table 2).

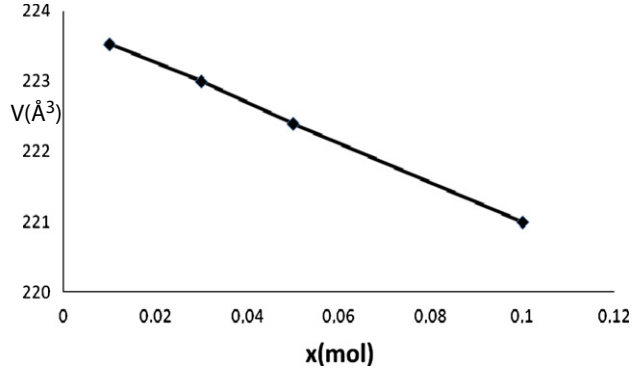

Fig. 3. Volume cell parameter of $Ca(Ti_{1-x}Cr_x)O_3$ perovskite powders versus x.

UV–vis–NIR spectra of powders and glazed samples are shown in Figs. 4 and 5. Cr^{4+} ions substituting in octahedral sites show an intense band centered at 520 nm and others show weak bands at 400, 700, 1000 and 1200 nm [11,12]. The following assignations can be made out: $^3A_{2g}(F)\rightarrow{}^3T_{2g}(F)$ 700 nm, $^3A_{2g}(F)\rightarrow{}^3T_{1g}(F)$ 520 nm, $^3A_{2g}(F)\rightarrow{}^3T_{1g}(P)$ 400 nm, $^1E_g(G)\rightarrow{}^1T_{2g}(G)$ 1000 nm and $^1E_g(G)\rightarrow{}^1T_{1g}(G)$ 1200 nm. The intense band at 520 nm is observed in all Cr–$CaTiO_3$ and Cr–$SrTiO_3$ powder samples in agreement with its pink shade that can be associated to Cr^{4+} ions substituting Ti^{4+} in octahedral sites. In the other hand this characteristic Cr^{4+} band is only detected for $x=0.01$ and 0.03 for Cr–$CaTiO_3$ and $x=0.01$ for Cr–$SrTiO_3$ glazed samples, indicating that the solid solutions of chromium in $CaTiO_3$ $x>0.03$ and in $SrTiO_3$ $x>0.01$ unstabilizes the perovskite lattice which is dissolved by the glaze.

UV–vis–NIR spectra of powders in Figs. 4 and 5 show two bands at 280 and 350–380 nm for Mg and Ca samples in the UV range, for Sr and Ba only a broad band centered at 350 nm is detected in this range. All these bands can be associated to three main parity-forbidden transitions of Cr^{3+} in octahedral coordination $^4A_2(^4F)\rightarrow{}^4T_2(^4F)$ at 600 nm and $^4A_2(^4F)\rightarrow{}^4T_1(^4F)$ at 400 nm, which overlap, and $^4A_2(^4F)\rightarrow{}^4T_2(^4P)$ at 250 nm which overlaps with $Ti^{4+}\leftrightarrow O^{2-}$ band transfer at 280 nm. In the visible range bands at 450 nm for Mg and 420 nm for Ba samples can be observed associated probably to $MgCr_2O_4$ spinel and barium chromate respectively. The weak bands at 650–700 nm can be assigned to Cr^{3+} spin-forbidden transitions $^4A_2(^4F)\rightarrow{}^2T_1(^2G)$ and $^4A_2(^4F)\rightarrow{}^2E(^2G)$ that overlaps and shifting to low wavelength from its position from Cr^{3+}–Ti^{4+} substitution in Cr-rutile due to the higher crystal field in the magnesium ilmenite or perovskite structure [13,14]. In the glazed samples an intense band centered at 250 nm is observed in all samples due to a transfer band associated to the glaze, also bands at 380–400 nm in the UV range and 600–700 nm in the visible bands can be observed and associated to Cr^{3+} transitions in octahedral coordination above described.

Fig. 6 is shown in order to emphasize the difference of UV–vis–NIR spectrum of Cr^{4+} in octahedral coordination (continuous line), of pink colored glazed samples with its characteristic band at 520 nm (more intense for Ca $x=0.01$ than in light pink of Sr $x=0.01$), and Cr^{3+} in octahedral coordination (dashed line), of light green colored glazed samples, with its characteristic band at 600 and 700 nm (also more intense for Ca $x=0.1$ than for Sr $x=0.1$).

The microstructure observed by SEM of representative powders is shown in Fig. 7. Aggregates of fine particles with a wide distribution between 2–10 μm can be observed in all cases (Fig. 7 left), but the size of the fine particles increases with the firing temperature (at 1200 °C particles of 1.5 μm can be observed for $x=0.1$ Cr–$CaTiO_3$ in Fig. 7a but little particles of 400 nm average size at 1000 °C for the $x=0.01$ Cr–$CaTiO_3$ in Fig. 6b, and decreases with the size

Table 1
XRD evolution of crystalline phases for samples $MTi_{0.9}Cr_{0.1}O_3$ with temperature. Crystalline phases and peak intensity considered (2θ position between parentheses): I (Ilmenite $MgTiO_3$, 33° 2θ) S (Spinel $MgCr_2O_4$, 18.5° 2θ), P (Periclase MgO,43° 2θ), K (Karrooite $MgTi_2O_5$, 25.5° 2θ), OP (Orthorhombic perovskite $CaTiO_3$,33° 2θ), CP (Cubic Perovskite $SrTiO_3$, 32.5° 2θ), TP (Tetragonal Perovskite $BaTiO_3$, 31.5° 2θ).

M	1000 °C	1200 °C
Mg	I(350)S(45)P(20)K(20)	I(450)S(45)
Ca	OP(290)$CaCrO_4$(15)	OP(330)
Sr	CP(850)$SrCrO_4$(25)	CP(750)
Ba	TP(430)$BaCrO_4$(20)	TP(380)$BaCrO_4$(30)

Table 2
CIEL*a*b* of indicated samples (interesting pink or green–yellow colors in bold).

Sample	T(°C)	x=0.01	x=0.03	x=0.05	x=0.1
$MgTi_{1-x}Cr_xO_3$					
Powder	**1000**	83.3/1.1/6.9	83.0/1.4/11.4	78.6/1.5/13.1	76.8/1.3/14.3
Glazed		74.6/3.6/7.6	73.6/0.2/6.2	68.6/1.0/5.9	60.7/3.8/10.5
Powder	**1200**	72.2/4.4/4.4	64.3/3.9/8.2	65.4/2.2/10.9	62.7/0.1/13.4
Glazed		72.8/2.3/4.9	68.3/0.4/6.8	65.5/−0.1/10.3	60.6/−0.9/14.5
$CaTi_{1-x}Cr_xO_3$					
Powder	**1000**	61.5/8.8/9.1	57.1/8.6/11.5	55.4/8.4/10.9	49.8/8.3/9.7
Glazed		63.2/11.9/1.2	64.2/8.2/2.9	63.4/2.4/2.6	65.2/−0.8/6.1
Powder	**1200**	**47.4/12.9/8.0**	**56.0/11.0/9.6**	**52.6/10.6/9.8**	**43.1/19.5/7.8**
Glazed		**55.5/14.7/−1.4**	**56.4/13.7/1.2**	69.8/−2.5/0.9	64.5/−5.1/6.4
$SrTi_{1-x}Cr_xO_3$					
Powder	**1000**	68.3/8.1/8.1	59.6/10.0/8.6	56.4/11.6/10.0	53.7/12.3/10.2
Glazed		66.2/6.3/11.9	65.1/−4.0/29.7	65.4/−1.3/31.8	65.8/1.3/30.7
Powder	**1200**	**59.1/10.8/7.4**	**52.8/11.8/7.9**	**52.9/11.8/9.6**	**50.2/12.0/9.9**
Glazed		**66.2/8.6/15.1**	65.2/0.2/22.7	64.9/4.6/16.5	**62.4/−0.9/29.3**
$BaTi_{1-x}Cr_xO_3$					
Powder	**1000**	79.2/−1.6/9.1	81.0/−1.5/11.4	82.0/−8.5/13.2	81.8/−4.1/17.2
Glazed		67.3/4.1/22.8	68.1/2.5/30.9	65.3/3.6/28.6	60.1/−0.1/47.9
Powder	**1200**	**50.1/5.6/9.4**	**51.5/5.2/9.9**	**56.6/5.0/11.7**	64.3/3.1/13.9
Glazed		**71.0/7.3/20.7**	**66.2/5.6/26.6**	67.9/3.7/30.6	**58.4/−1.1/43.9**

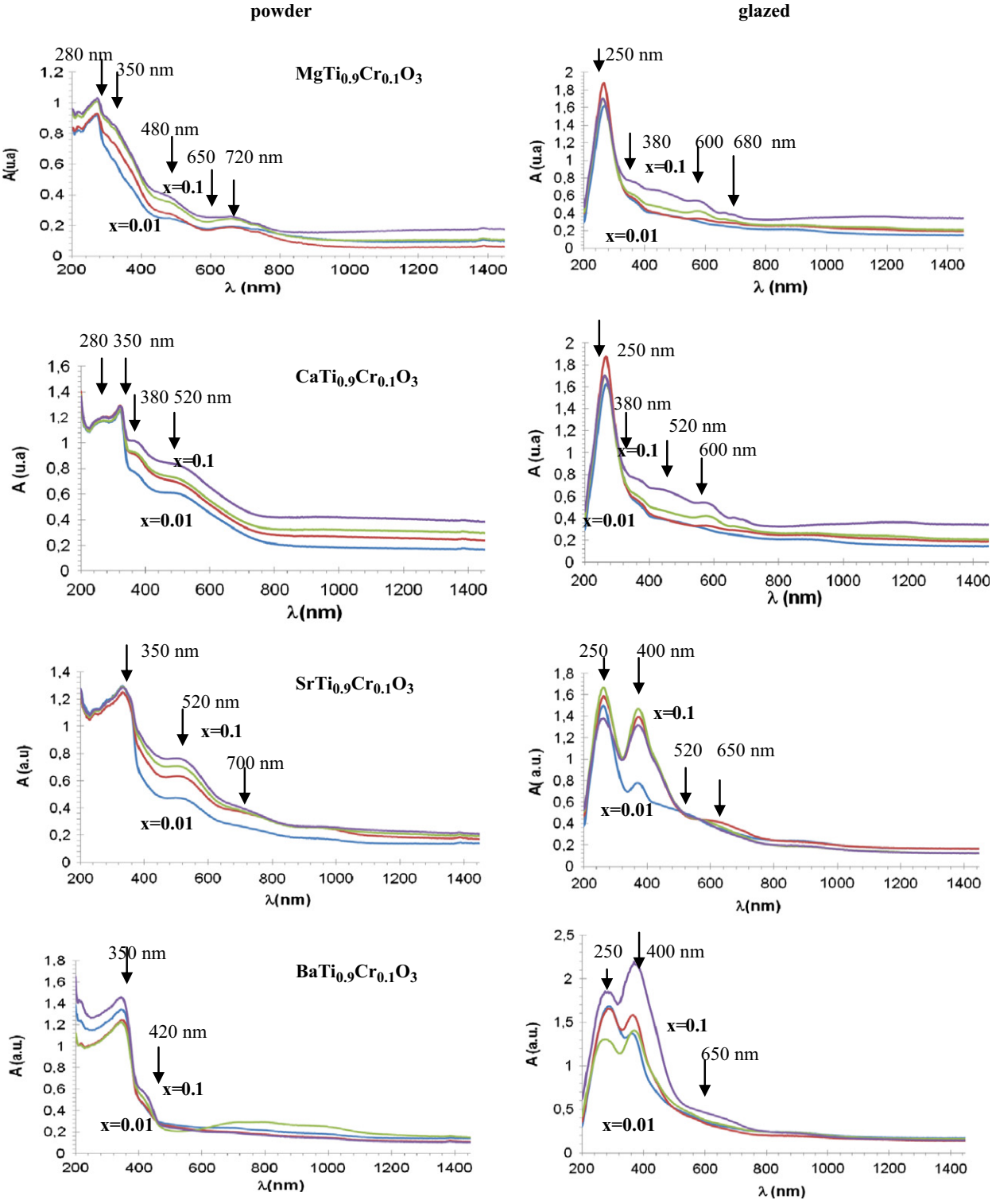

Fig. 4. UV–vis–NIR of samples fired at 1000 °C.

of alkaline earth cation (particles of 400 nm average size at 1000 °C for the $x=0.01$ Cr–$SrTiO_3$ in Fig. 7c).

4. Conclusions

The reactivity, structure, limit of solid solution, stability and pigmenting properties of chromium doped $M(Cr_xTi_{1-x})O_3$ M = Mg, Ca, Sr, Ba solid solutions depends of the M cation: (a) Cr–$MgTiO_3$ crystallizes magnesium ilmenite $MgTiO_3$ (SG = R-3) together very weak peaks associated to $MgCr_2O_4$ spinel when fired at 1200 °C inhibiting the Cr entrance in ilmenite lattice and do not show pigmenting properties in ceramic glazes, (b) Cr–$CaTiO_3$ crystallizes orthorhombic perovskite (SG = Pbnm) pink solid solutions ($a^* > 10$)

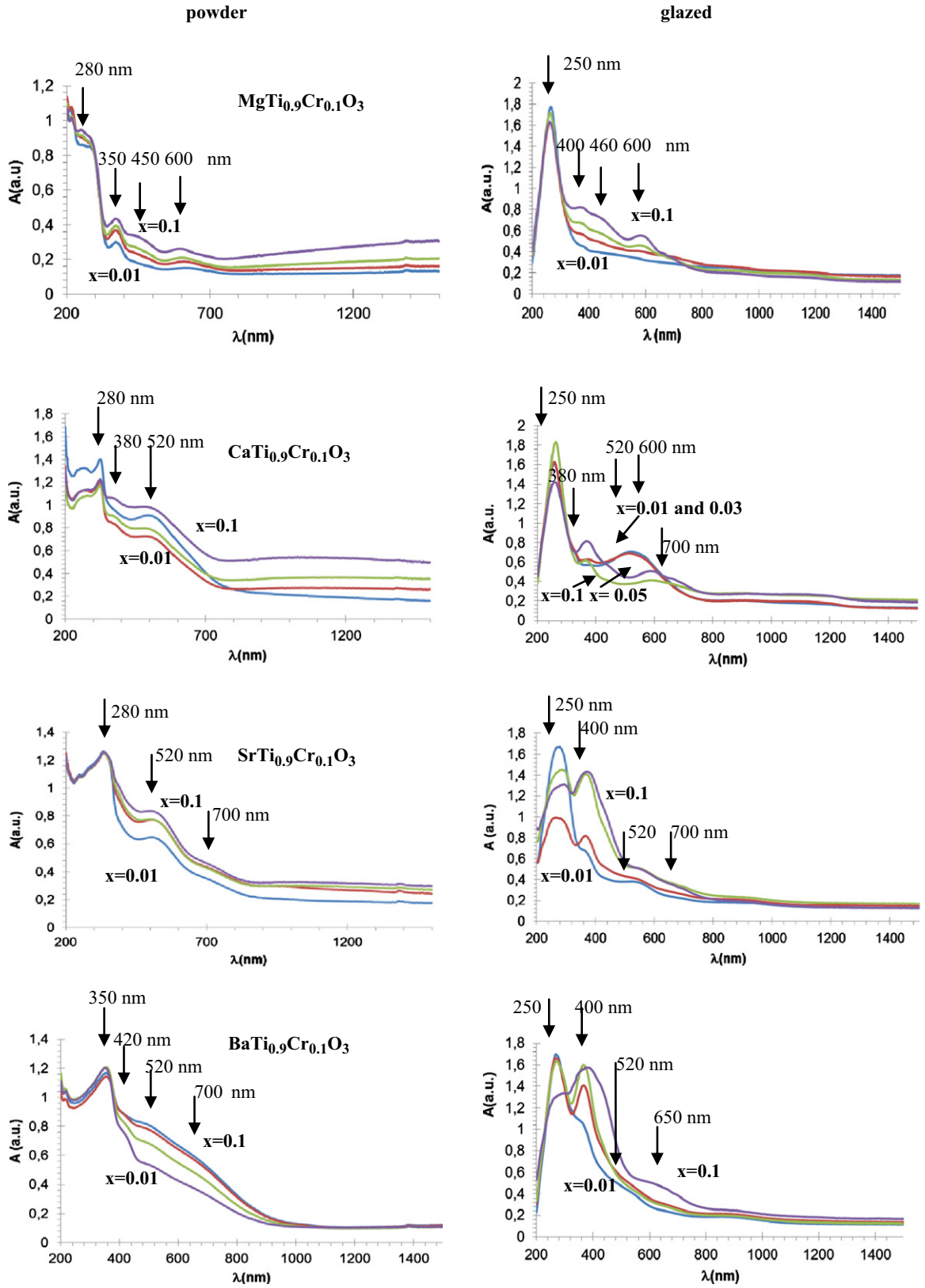

Fig. 5. UV–vis–NIR of samples fired at 1200 °C.

associated to Cr^{4+} substituting Ti^{4+} in the optical spectra which above $x=0.03$ unstabilizes in glazes and produce light green shades, (c) Cr–$SrTiO_3$ crystallizes ideal cubic perovskite (SG=Pm3m) pink solid solutions that unstabilizes in glazes and the pink color is observed only for $x=0.01$, at higher x values Cr–$SrTiO_3$ produces yellow

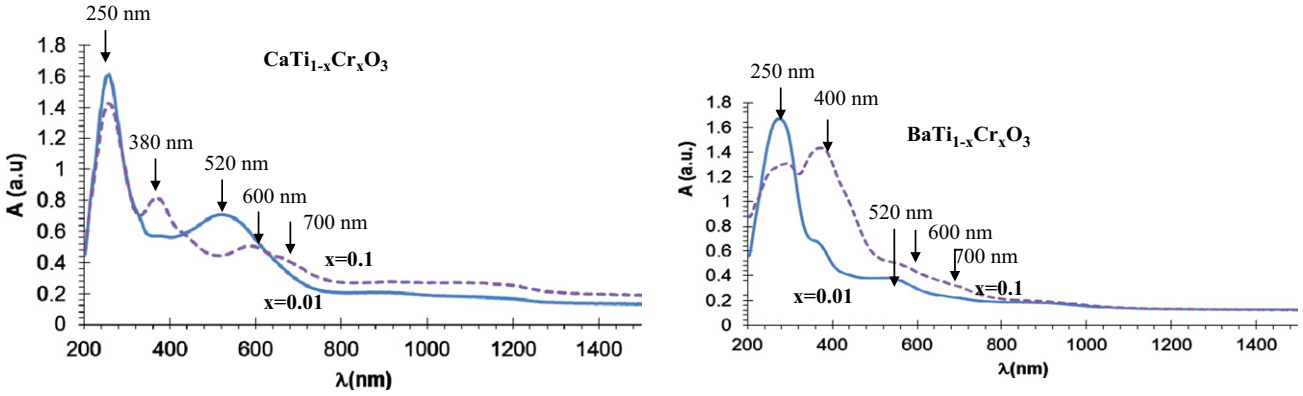

Fig. 6. UV–vis–NIR spectra of Cr^{4+} in octahedral coordination (continuous line in both Ca and Sr samples $x=0.01$) and of Cr^{3+} in octahedral coordination (dashed line of same samples $x=0.1$).

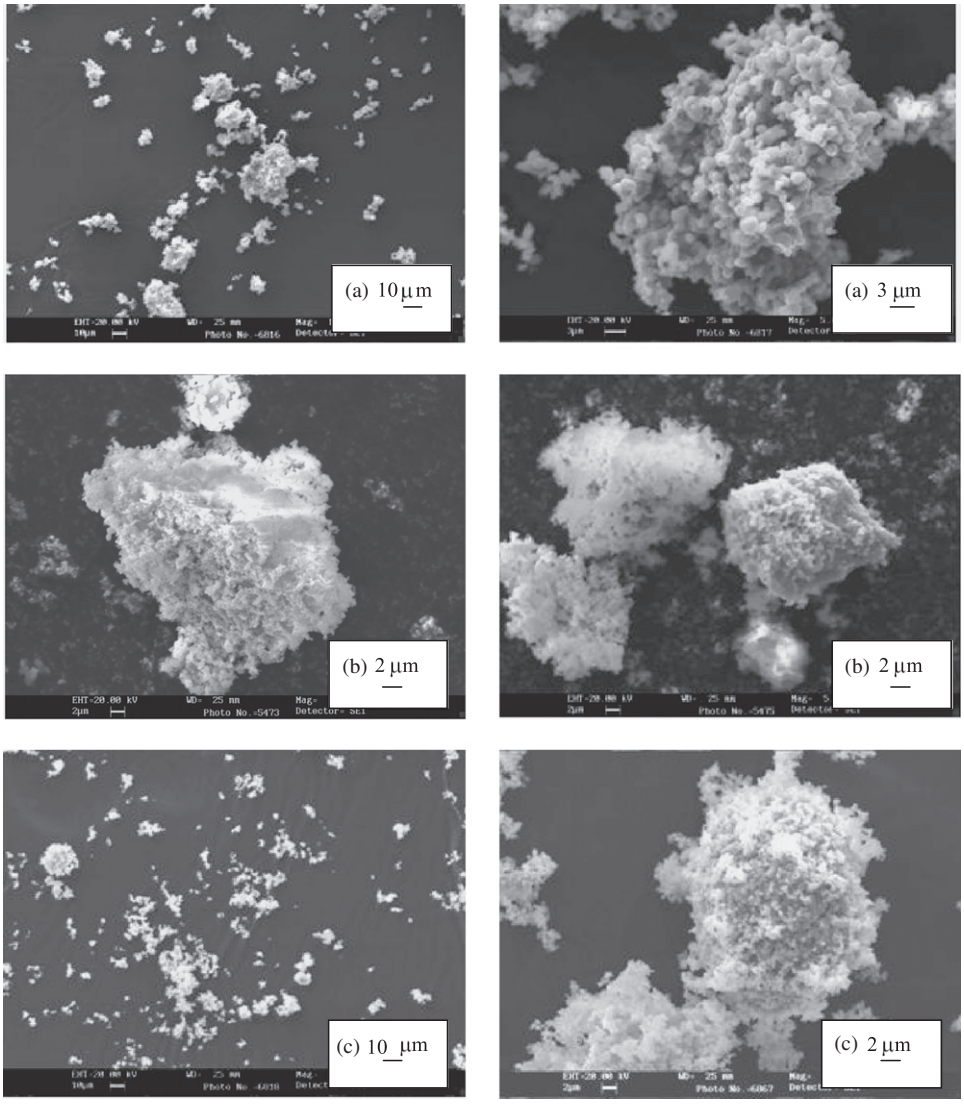

Fig. 7. SEM micrographs of representative powders: (a) Cr–$CaTiO_3$ $x=0.1$ fired at 1200 °C, (b) Cr–$CaTiO_3$ $x=0.01$ fired at 1000 °C and (c) Cr–$SrTiO_3$ $x=0.01$ fired at 1200 °C.

color in glazes, and (d) Cr–$BaTiO_3$ crystallizes tetragonal perovskite (SG=P4mn) at 1200 °C with residual peaks associated to $BaCrO_4$ at $x=0.1$ which are light pink (a^* around 5) until $x=0.05$ and only until $x=0.03$ the Cr^{4+}–Ti^{4+} solid solution is stable in glazes, at higher x values Cr–$BaTiO_3$ produces intense green–yellow color in

glazes. All powders show aggregates (between 2–10 μm of average size) of fine particles (between 200–1000 nm of average size).

Acknowledgements

Authors acknowledge the financial support given by Fundacion Caja Castellón-UJI, P1-1B2010-09 Project.

References

[1] M. Johnsson, P. Lemmens, Crystallography and Chemistry of Perovskites, in: H. Kronmüller (Ed.), Handbook of Magnetism and Advanced Magnetic Media, John Wiley & Sons, New York, 2006.
[2] K. Leinenweber, W. Utsumi, Y. Tsuchida, T. Yagi, K. Kurita, Physics and Chemistry of Minerals 18 (1991) 244–250.
[3] A. Navrotsky, Energetics and crystal chemical systematics among ilmenite, lithium niobate and perovskite structures, Chemistry of Materials 10 (1998) 2787–2794.
[4] C. Gargori, R. Galindo, M. Llusar, S. Cerro, A. García, G. Monrós, Chromium–calcium titanate red ceramic pigment, Advances in Science and Technology 68 (2010) 208–212.
[5] C. Gargori, S. Cerro, R. Galindo, A. García, M. Llusar, J. Badenes, G. Monrós, New vanadium doped calcium titanate ceramic pigment, Ceramics International, Ceramics International 37 (2011) 3665–3670.
[6] C. Gargori, S. Cerro, R. Galindo, A. García, M. Llusar, G. Monrós, Iron and chromium doped perovskite ($CaMO_3$ M = Ti, Zr) ceramic pigments, effect of mineralizer, Ceramics International 38 (2012) 4453–4460.
[7] R.D. Shannon, Revised effective ionic radii and systematic studies of interatomic distances in halides and chalcogenides, Acta Crystallographica A32 (1976) 751–767.
[8] POWCAL and LSQC programmes, Department of Chemistry, University of Aberdeen, UK.
[9] C.I.E. Commission International de l'Eclairage, Recommendations on Uniform Color Spaces, Color Difference Equations, Psychometrics Color Terms, Supplement no. 2 of CIE Pub. no. 15 (E1–1.31) 1971, Bureau Central de la CIE, Paris, 1978.
[10] L. Vegard, Die Konstitution der Mischkristalle und die Raumfüllung der Atome, Zeitschrift für Physik 5 (1921) 17–22.
[11] F. Matteucci, C. Lepri Neto, M. Dondi, G. Cruciani, G. Baldi, A.O. Boschi, Colour development of red perovskite pigment $Y(Al,Cr)O_3$ in various ceramic applications, Advances in Applied Ceramics 105 (2) (2006) 99–106.
[12] G. Monrós, H. Pinto, J. Badenes, M. Llusar, M.A. Tena, Chromium(IV) stabilisation in new ceramic matrices by co-precipitation method: application as ceramic pigments, Zeitschrift Fur Anorganische Und Allgemeine Chemie 631 (2005) 2131–2135.
[13] (a) F. Matteucci, G. Cruciani, M. Dondi, M. Raimondo, The role of counter ions (Mo, Nb, Sb, W) in Cr-, Mn-, Ni- and V-doped rutile ceramic pigments part 1. Crystal structure and phase transformations, Ceramics International 32 (4) (2006) 385–392.
(b) M. Dondi, G. Cruciani, G. Guarini, F. Matteucci, M. Raimondo, The role of counter ions (Mo, Nb, Sb, W) in Cr-, Mn-, Ni- and V-doped rutile ceramic pigments part 2, Colour and technological properties, Ceramics International, 32 (4) 393–405.
[14] (a) S. Ishida, M. Hayashi, Y. Fujimura, K. Fujiyoshi, Spectroscopic study of the chemical state and coloration of chromium in rutile, Journal of the American Ceramic Society 73 (11) (1990) 3351–3355.
(b) A.B. Lever, Studies in Physical and Theoretical Chemistry Inorganic Electronic Spectroscopy, vol. 3, Elsevier, Amsterdam, 1986.